Monthly Notices
of the
ROYAL ASTRONOMICAL SOCIETY

MNRAS **466,** 2085–2098 (2017)
Advance Access publication 2016 December 11

doi:10.1093/mnras/stw3225

Light-curve and spectral properties of ultrastripped core-collapse supernovae leading to binary neutron stars

Takashi J. Moriya,[1,2]★ Paolo A. Mazzali,[3,4] Nozomu Tominaga,[5,6] Stephan Hachinger,[7] Sergei I. Blinnikov,[8,9,6] Thomas M. Tauris,[10,2] Koh Takahashi,[11] Masaomi Tanaka,[1,6] Norbert Langer[2] and Philipp Podsiadlowski[12,2]

[1]*Division of Theoretical Astronomy, National Astronomical Observatory of Japan, National Institutes of Natural Sciences, 2-21-1 Osawa, Mitaka, Tokyo 181-8588, Japan*
[2]*Argelander Institute for Astronomy, University of Bonn, Auf dem Hügel 71, D-53121 Bonn, Germany*
[3]*Astrophysics Research Institute, Liverpool John Moores University, IC2, Liverpool Science Park, 146 Browlow Hill, Liverpool L3 5RF, UK*
[4]*Max Planck Institute for Astrophysics, Karl-Schwarzschild-Straße 1, D-85748 Garching, Germany*
[5]*Department of Physics, Faculty of Science and Engineering, Konan University, 8-9-1 Okamoto, Kobe, Hyogo 658-8501, Japan*
[6]*Kavli Institute for the Physics and Mathematics of the Universe (WPI), The University of Tokyo Institutes for Advanced Study, The University of Tokyo, 5-1-5 Kashiwanoha, Kashiwa, Chiba 277-8583, Japan*
[7]*Leibniz Supercomputing Centre (LRZ), Bavarian Academy of Sciences and Humanities, Boltzmannstraße 1, D-85748 Garching, Germany*
[8]*Institute for Theoretical and Experimental Physics, Bolshaya Cheremushkinskaya ulitsa 25, 117218 Moscow, Russia*
[9]*All-Russia Research Institute of Automatics, Sushchevskaya ulitsa 22, 127055 Moscow, Russia*
[10]*Max Planck Institute for Radio Astronomy, Auf dem Hügel 69, D-53121 Bonn, Germany*
[11]*Department of Astronomy, Graduate School of Science, The University of Tokyo, Hongo 7-3-1, Bunkyo, Tokyo 113-0033, Japan*
[12]*Department of Physics, University of Oxford, Denys Wilkinson Building, Keble Road, Oxford OX1 3RH, UK*

Accepted 2016 December 8. Received 2016 December 8; in original form 2016 August 25

ABSTRACT

We investigate light-curve and spectral properties of ultrastripped core-collapse supernovae. Ultrastripped supernovae are the explosions of heavily stripped massive stars that lost their envelopes via binary interactions with a compact companion star. They eject only $\sim$0.1 $M_\odot$ and may be the main way to form double neutron-star systems that eventually merge emitting strong gravitational waves. We follow the evolution of an ultrastripped supernova progenitor until iron core collapse and perform explosive nucleosynthesis calculations. We then synthesize light curves and spectra of ultrastripped supernovae using the nucleosynthesis results and present their expected properties. Ultrastripped supernovae synthesize $\sim$0.01 $M_\odot$ of radioactive ^{56}Ni, and their typical peak luminosity is around 10^{42} erg s^{-1} or -16 mag. Their typical rise time is 5–10 d. Comparing synthesized and observed spectra, we find that SN 2005ek, some of the so-called calcium-rich gap transients, and SN 2010X may be related to ultrastripped supernovae. If these supernovae are actually ultrastripped supernovae, their event rate is expected to be about 1 per cent of core-collapse supernovae. Comparing the double neutron-star merger rate obtained by future gravitational-wave observations and the ultrastripped supernova rate obtained by optical transient surveys identified with our synthesized light-curve and spectral models, we will be able to judge whether ultrastripped supernovae are actually a major contributor to the binary neutron-star population and provide constraints on binary stellar evolution.

Key words: gravitational waves – supernovae: general – supernovae: individual: PTF10iuv – supernovae: individual: SN 2005ek – supernovae: individual: SN 2010X.

1 INTRODUCTION

Multiplicity of massive stars plays an essential role in determining stellar structure at the time of their core collapse and thus their supernova (SN) properties (e.g. Langer 2012; Vanbeveren & Mennekens 2015; Yoon 2015; Marchant et al. 2016). In particular, the lack of hydrogen-rich layers in progenitors of stripped-envelope core-collapse SNe (i.e. Type IIb/Ib/Ic SNe) is often suggested to be caused by binary interaction (e.g. Wheeler & Levreault 1985; Ensman & Woosley 1988; Podsiadlowski, Joss & Hsu 1992; Nomoto et al. 1994; Shigeyama et al. 1994; Woosley et al. 1994; Bersten

★ E-mail: takashi.moriya@nao.ac.jp.

et al. 2012, 2014; Fremling et al. 2014; Ergon et al. 2015; Eldridge et al. 2015; Lyman et al. 2016a). The small typical ejecta mass estimated from light curves (LCs) of stripped-envelope SNe ($\simeq$ 1–5 $M_\odot$; e.g. Sauer et al. 2006; Drout et al. 2011; Taddia et al. 2015; Lyman et al. 2016a), and nucleosynthetic signatures estimated from their spectral modelling (e.g. Jerkstrand et al. 2015), support progenitors with relatively small zero-age main sequence (ZAMS) masses. The less massive ZAMS mass stars need to remove their hydrogen-rich envelopes with mass-loss caused by binary interactions because of their inefficient radiation-driven wind (e.g. Podsiadlowski et al. 1992, 2004a; Nomoto, Iwamoto & Suzuki 1995; Izzard, Ramirez-Ruiz & Tout 2004; Yoon, Woosley & Langer 2010; Eldridge, Langer & Tout 2011; Benvenuto, Bersten & Nomoto 2013; Eldridge & Maund 2016; Lyman et al. 2016a). It is also known that mass-loss caused by binary interaction is essential to explain the observational ratio of stripped-envelope SNe to hydrogen-rich SNe (e.g. Eldridge, Izzard & Tout 2008; Smith et al. 2011; Eldridge et al. 2013).

Some Type Ib/Ic SNe are known to have a much faster LC evolution than others. While typical Type Ib/Ic SNe reach their peak luminosity in $\sim$20 d (e.g. Drout et al. 2011; Prentice et al. 2016), rapidly evolving SN LCs rise in less than $\sim$10 d and decline quickly on a similar time-scale (e.g. Kasliwal et al. 2010, 2012; Kawabata et al. 2010; Ofek et al. 2010; Perets et al. 2010; Poznanski et al. 2010; Drout et al. 2013, 2014; Inserra et al. 2015). The simplest way to interpret the rapid LC evolution of some Type Ib/Ic SNe is that their ejecta mass is much smaller than in the more slowly evolving SNe (see also, e.g. Drout et al. 2014; Kleiser & Kasen 2014; Tanaka et al. 2016). LC evolution becomes faster with smaller ejecta mass because of the smaller diffusion time-scale. This is roughly proportional to $(M_{\rm ej}^3/E_{\rm ej})^{1/4}$, where $M_{\rm ej}$ is the ejecta mass and $E_{\rm ej}$ is the kinetic energy (e.g. Arnett 1982). The ejecta mass of rapidly evolving SNe is typically estimated to be $\sim$0.1 $M_\odot$, which is an order of magnitude smaller than that of typical Type Ib/Ic SNe (e.g. Poznanski et al. 2010; Kasliwal et al. 2012; Drout et al. 2013).

Type Ib/Ic SNe with rapidly evolving LCs show diversity in their peak luminosities and spectra. SN 2002bj is among the first observed rapidly evolving Type Ib/Ic SNe and among the brightest with its peak magnitude at around $-$18 mag (Poznanski et al. 2010). Many rapidly evolving SNe have their peak magnitudes at around $-$16 mag with different spectral properties. One example of rapidly evolving SNe in this luminosity range is so-called Ca-rich gap transients. They are optical transients whose peak luminosity lie between that of classical novae and SNe, and they show strong Ca lines especially in the nebular phase (e.g. Kasliwal et al. 2012). Although they are called Ca-rich transients, they may not necessarily be Ca-rich. What is indicated from their spectra is that they have a larger fraction of Ca to O than typical Type Ib/Ic SNe. Several progenitor scenarios have been suggested for these events (e.g. Kawabata et al. 2010; Perets et al. 2010), but their nature is not yet clear. There also exist rapidly evolving SNe with similar luminosities to the Ca-rich gap transients but with very different spectral features such as SN 2005ek (Drout et al. 2013) and SN 2010X (Kasliwal et al. 2010). Another kind of rapidly evolving SNe are SN 2002cx-like SNe, which are also known as Type Iax SNe; they are characterized by their strong Si and S features with relatively low photospheric velocities and by the wide peak luminosity range covering from $\sim-$ 14 to $\sim-$ 19 mag (e.g. Foley et al. 2013).

A number of possibilities have been suggested to obtain a small ejecta mass to explain the rapidly evolving SNe, including some not related to the core collapse of massive stars (e.g. Kitaura, Janka & Hillebrandt 2006; Moriya et al. 2010; Shen et al. 2010; Kleiser & Kasen 2014; Dessart & Hillier 2015; Kashiyama & Quataert 2015; Moriya & Eldridge 2016). In particular, Tauris et al. (2013) and Tauris, Langer & Podsiadlowski (2015) proposed an 'ultrastripped' core-collapse SN scenario to explain small ejecta masses. They showed that tight helium star–neutron star (NS) binary systems, presumably created in the common-envelope phase from high-mass X-ray binaries (Tauris & van den Heuvel 2006), can lead to the extreme stripping of the helium envelope and result in SNe with ejecta masses of the order of 0.1 $M_\odot$ or less. The SN ejecta mass from these systems is even less than those typically obtained in SN progenitors from the first exploding stars ($\sim$1 $M_\odot$) during binary evolution (e.g. Yoon et al. 2010; Lyman et al. 2016a).

Several studies have investigated the observational properties of stripped-envelope SNe with ejecta larger than 1 $M_\odot$ coming from progenitors obtained from binary stellar evolution (e.g. Dessart et al. 2015). However, few LC and spectral studies have been carried out for ultrastripped SNe. A previous study of ultrastripped SNe (Tauris et al. 2013) only provided LC models. Because there are several proposed ways to make SNe with rapidly evolving LCs, LC information is not sufficient to identify ultrastripped SNe observationally. In addition, the ^{56}Ni mass was treated as a free parameter in the previous study. In this paper, we investigate not only LCs but also spectral properties of ultrastripped SNe by performing explosive nucleosynthesis calculations that provide an appropriate estimate for the ^{56}Ni mass synthesized during the explosion, so that we can have a better understanding of their observational signatures and identify ultrastripped SNe observationally.

Ultrastripped SNe are closely connected to the formation of double NS systems. It was argued by Tauris et al. (2013, 2015) that *all* double NS systems formed in the Galactic disc (i.e. outside dense environments such as globular clusters) that are tight enough to merge within a Hubble time *must* have been produced from an ultrastripped SN. Therefore, ultrastripped SNe are related to sources of gravitational waves (GW) detected by LIGO (e.g. Abadie et al. 2010). In addition, double NS systems that merge are suggested to cause short gamma-ray bursts (Blinnikov et al. 1984; Paczynski 1986; Narayan, Paczynski & Piran 1992) and *r*-process element nucleosynthesis (e.g. Rosswog et al. 1999; Argast et al. 2004; Hirai et al. 2015), possibly followed by a so-called kilonova (e.g. Metzger et al. 2010; Barnes & Kasen 2013; Tanaka & Hotokezaka 2013). However, to produce a double NS system a massive binary must survive two SN explosions. A binary system is likely to be disrupted by the first SN explosion because of a combination of sudden mass-loss and a kick imparted to the newborn NS (Brandt & Podsiadlowski 1995). Ultrastripped SNe, on the other hand, eject very little mass and are unlikely to have large NS kicks in general because of their rapid explosions (Podsiadlowski et al. 2004b; Suwa et al. 2015; Tauris et al. 2015). Thus, ultrastripped SNe avoid these two major obstacles in forming double NS systems and are therefore likely to produce systems that lead to merger events if the post-SN orbital period is short enough. Future constraints on the observed rate of ultrastripped SNe can be directly compared to the double NS merger rate determined from GW observations (Tauris et al. 2015). This can be used to verify their evolutionary connection. The merger rate of double NS systems will be known within a few years when LIGO/VIRGO reach full design sensitivity. We refer to Abadie et al. (2010), Berry et al. (2015) and Abbott et al. (2016b) for detailed reviews on the expected merger rates.

This paper is organized as follows. Section 2 presents the numerical methods we adopt in our study. Our synthetic LC and spectral models are presented in Section 3. We compare our results with

observations in Section 4. We discuss our results in Section 5 and conclude this paper in Section 6.

2 METHOD

2.1 Progenitor

We investigate the observational properties of explosions originating from the ultrastripped SN progenitor presented in Tauris et al. (2013, see also Tauris et al. 2015). This is a typical model of ultrastripped SNe. The total progenitor mass at explosion is 1.50 $M_\odot$ with a carbon+oxygen core of 1.45 $M_\odot$. The helium ZAMS mass of the progenitor was 2.9 $M_\odot$. Tauris et al. (2013) evolved the progenitor until shortly after the onset of off-centre oxygen burning using the BEC binary stellar evolution code (Heger et al. 2000; Yoon et al. 2010; Brott et al. 2011 and references therein). Although the remaining time to collapse is estimated to be about 10 yr and the final progenitor mass does not change until the collapse, the density in the inner layers of the progenitor increases significantly in the remaining time. As the final density structure is critical for the explosive nucleosynthesis results, we need to follow the progenitor evolution until core collapse. The BEC code is not suitable for this.

In order to obtain an SN progenitor evolved until core collapse, we therefore used the public stellar evolution code MESA (Paxton et al. 2011, 2013, 2015). We used the same physical parameters as in the Tauris et al. (2013) BEC calculations in MESA. In particular, we used a mixing length parameter of 2 with a semiconvection efficiency parameter of 1. As the core mass is rather small, weak reactions play an important role in the evolution of the core approaching collapse (e.g. Jones et al. 2013; Takahashi, Yoshida & Umeda 2013; Schwab, Quataert & Bildsten 2015). Therefore, we used the large nuclear network `'mesa151.net'` provided in MESA, which includes 151 nuclei up to ^{65}Ni with important weak reactions such as electron capture by ^{33}S and ^{35}Cl. We stopped the calculation when the stellar core started to infall with a speed of 1000 km s^{-1}.

First, we evolved a star starting from the helium ZAMS as is done by Tauris et al. (2013), but as a single star. Because the mass lost by the binary interactions like Roche lobe overflow is known from the binary calculation of Tauris et al. (2013), we imposed their mass-loss in our single-star evolution calculation. Thus, our single-star evolution calculation takes mass-loss caused by binary stellar evolution into account in a simplified way. Tauris et al. (2013) obtained a 1.50 $M_\odot$ helium star with a carbon+oxygen core of 1.45 $M_\odot$ from a helium ZAMS star of 2.90 $M_\odot$ that suffers from Roche lobe overflow to an NS with initial orbital period of 0.1 d. We slightly increased the initial helium mass to 2.949 $M_\odot$ in order to obtain the same carbon+oxygen core mass after the core helium burning in our MESA calculation. The evolution of the central density and temperature is presented in Fig. 1 . We find that the internal evolution of our progenitor is essentially the same as that in Tauris et al. (2013) up to the point they succeeded to follow. The star forms an Fe core and collapses as was presumed by Tauris et al. (2013, 2015). It is suggested that low-mass core-collapse SN progenitors experience violent silicon flashes shortly before the core collapse (Woosley & Heger 2015), but we do not find such a flash in our model. If such a flash occurs, it may result in a creation of a dense helium-rich circumstellar medium around the progenitor and the SN may be observed as Type Ibn (e.g. Moriya & Maeda 2016).

The final density structure of the progenitor at collapse is presented in Fig. 2. The abundance of the Fe-group elements sharply increases at an enclosed mass of 1.35 $M_\odot$, while the electron fraction sharply decreases there. Thus, we estimate that the final

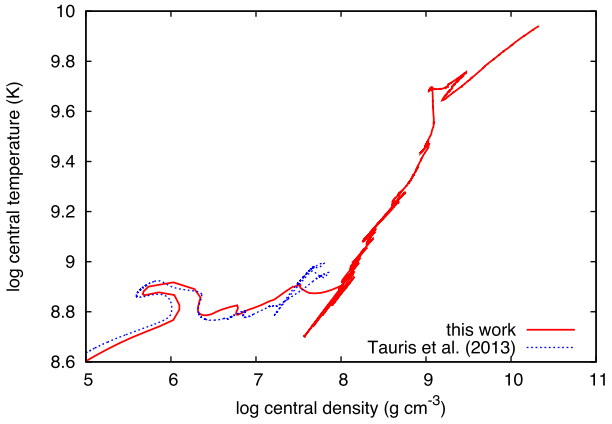

Figure 1. Evolution of the central density and temperature of our ultrastripped SN progenitor obtained with MESA. We also present the central density and temperature evolution obtained by Tauris et al. (2013) with BEC.

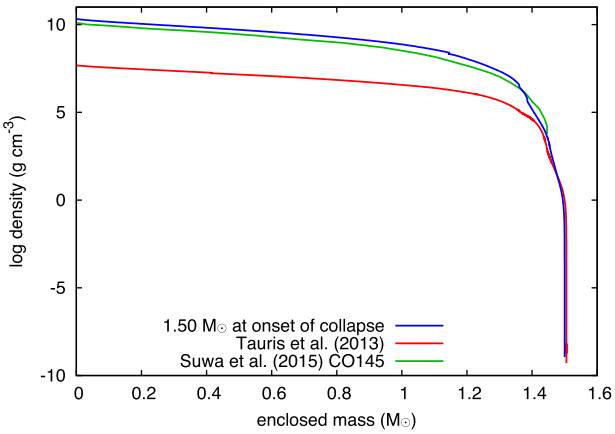

Figure 2. Progenitor density structure at core collapse. We also show the density structure from the model of Tauris et al. (2013) that is shortly after off-centre oxygen ignition, some ∼10 yr prior to core collapse. We show the density structure at the collapse from Suwa et al. (2015) from the progenitor having the same carbon+oxygen core mass of 1.45 $M_\odot$ as our model.

iron-core mass at the time of collapse is 1.35 $M_\odot$. This iron-core mass is comparable to that obtained recently by Suwa et al. (2015, 1.33 $M_\odot$) from a progenitor model with a similar carbon+oxygen core mass as ours (1.45 $M_\odot$). We compare our progenitor with that of Suwa et al. (2015) in Fig. 2. The internal structure of the collapsing models is similar. We also show for comparison the density structure obtained with the BEC code at a time ∼10 yr prior to core collapse.

2.2 Nucleosynthesis

The collapsing progenitor described in the previous section was then used to follow the explosive nucleosynthesis. Numerical calculations of explosive nucleosynthesis were performed with the same numerical code as in previous studies of explosive nucleosynthesis in core-collapse SNe (e.g. Nakamura et al. 2001; Tominaga, Umeda & Nomoto 2007). It is a one-dimensional explicit Lagrangian hydrodynamics code in which a piece-wise parabolic method is adopted (Colella & Woodward 1984). The α-network is coupled with hydrodynamics and detailed nucleosynthesis calculations are performed as post-processing modelling. We used a reaction network including 280 isotopes up to ^{79}Br (table 1 in Umeda & Nomoto 2005).

Table 1. Explosive nucleosynthesis results of the 1.50 $M_\odot$ model for different ejecta masses and explosion energies. Mass fractions at the end of the nucleosynthesis calculations are presented. The value in each column, a (x), means that the corresponding mass fraction is $a \times 10^x$. The abundance estimated for SN 2005ek based on its peak spectrum (Drout et al. 2013) is also shown. T_{max} is the maximum temperature reached during the explosive nucleosynthesis calculations.

Element	$M_{ej} = 0.20\,M_\odot$			$M_{ej} = 0.15\,M_\odot$			SN 2005ek
	0.50 B	0.25 B	0.10 B	0.50 B	0.25 B	0.10 B	
He	2.4 (−1)	2.3 (−1)	2.2 (−1)	3.0 (−1)	2.9 (−1)	2.8 (−1)	–
C	4.3 (−2)	4.5 (−2)	4.7 (−2)	5.8 (−2)	6.0 (−2)	6.3 (−2)	2.0 (−2)
O	1.7 (−1)	1.8 (−1)	1.9 (−1)	2.3 (−1)	2.4 (−1)	2.5 (−1)	8.6 (−1)
Ne	5.2 (−2)	6.9 (−2)	7.9 (−2)	7.0 (−2)	9.2 (−2)	1.1 (−1)	–
Mg	2.3 (−2)	2.5 (−2)	2.6 (−2)	3.0 (−2)	3.4 (−2)	3.5 (−2)	8.2 (−2)
Si	5.1 (−2)	5.3 (−2)	6.0 (−2)	6.7 (−2)	7.0 (−2)	8.0 (−2)	2.5 (−2)
S	2.4 (−2)	2.5 (−2)	2.3 (−2)	3.2 (−2)	3.4 (−2)	4.0 (−2)	8.0 (−3)
Ca	3.9 (−3)	4.4 (−3)	5.1 (−3)	5.2 (−3)	5.8 (−3)	6.7 (−3)	1.2 (−3)
Sc	1.0 (−6)	1.0 (−6)	3.4 (−7)	4.3 (−7)	1.1 (−6)	3.8 (−7)	–
Ti	1.3 (−4)	7.2 (−5)	2.8 (−5)	1.3 (−4)	7.8 (−5)	3.1 (−5)	3.3 (−4)
V	3.2 (−6)	5.8 (−6)	2.4 (−6)	2.4 (−6)	6.6 (−6)	2.8 (−6)	–
Cr	2.7 (−4)	2.2 (−4)	1.9 (−4)	3.0 (−4)	2.6 (−4)	2.4 (−4)	3.3 (−4)
Mn	1.9 (−5)	2.6 (−5)	2.8 (−5)	2.4 (−5)	3.4 (−5)	3.8 (−5)	–
Fe	3.3 (−3)	4.3 (−3)	6.0 (−3)	4.3 (−3)	5.7 (−3)	8.0 (−3)	1.5 (−3)
Co	2.8 (−4)	4.0 (−4)	5.8 (−4)	3.7 (−4)	5.3 (−4)	7.7 (−4)	1.2 (−3)
^{56}Ni mass	0.034 $M_\odot$	0.030 $M_\odot$	0.026 $M_\odot$	0.031 $M_\odot$	0.027 $M_\odot$	0.021 $M_\odot$	0.03 $M_\odot$
$T_{max}/10^9$ K	14	12	11	7.5	6.6	6.0	–

2.3 Explosive hydrodynamics and LCs

Synthetic LCs were numerically obtained using the one-dimensional multigroup radiation hydrodynamics code STELLA (Blinnikov & Bartunov 1993; Blinnikov et al. 1998, 2006; Blinnikov & Sorokina 2004; Baklanov, Blinnikov & Pavlyuk 2005; Sorokina et al. 2015). STELLA has been used to model SN LCs of various kinds, including ultrastripped SNe (Tauris et al. 2013). We take the progenitor structure above a mass cut and inject thermal energy at the bottom of the structure to initiate the explosion. The amount of thermal energy injected is $E_{ej} + E_{bind}$, where E_{bind} is the total binding energy of the progenitor. We used the chemical composition obtained from explosive nucleosynthesis.

We show LC and spectral models obtained using two different mass cuts, at 1.30 and 1.35 $M_\odot$, respectively. A mass cut of 1.35 $M_\odot$ corresponds to the final iron-core mass of the progenitor model. Suwa et al. (2015) obtained a final NS baryonic mass of 1.35 $M_\odot$ from an explosion using the same carbon+oxygen core mass. Tauris et al. (2013) used a mass cut of 1.30 $M_\odot$. Both the small Fe core mass of our progenitor model and simulations by Suwa et al. (2015) suggest that the mass cut is likely to be small.

2.4 Spectra

The spectral properties of ultrastripped SNe have been investigated using the Monte Carlo spectral synthesis code developed by Mazzali & Lucy (1993). We refer to Mazzali & Lucy (1993), Lucy (1999), Mazzali (2000) and Tanaka et al. (2011) for details. This code has been used for many SN spectral synthesis studies (e.g. Mazzali, Lucy & Butler 1992; Mazzali et al. 1993; Mazzali, Iwamoto & Nomoto 2000; Mazzali et al. 2001; Tanaka et al. 2011).

The code is applicable in early phases of SNe when a photosphere exists in the ejecta from where photons are assumed to be emitted with a blackbody spectrum. The code requires a density structure, abundances, position of the photosphere and emerging SN luminosity to synthesize spectra. We used the average abundances of the models obtained from the nucleosynthesis calculations (Table 1) in our spectral modelling. We did not assume stratification of chemical elements in the SN ejecta because the ejecta mass is small and the ejecta are likely to be well mixed (e.g. Hachisu et al. 1991). We took the density structure and luminosity from STELLA. The spectral code assumes homologous expansion of the SN ejecta, which is satisfied in every model we present in this paper. A converging model is obtained by changing photospheric velocity and temperature in the spectral synthesis code.

Our models contain a large fraction of helium, and some rapidly evolving SNe are of Type Ib. However, the code we mainly use does not include non-thermal excitation of helium that is essential in modelling helium features in SN spectra (e.g. Lucy 1991; Mazzali & Lucy 1998; Hachinger et al. 2012). We investigate the effect of non-thermal helium excitation using a code developed by Hachinger et al. (2012) and find that non-thermal excitation does not have a strong effect on the spectra we present in this study (Section 3.3.3).

3 RESULTS

3.1 Nucleosynthesis

We calculated explosive nucleosynthesis for three different explosion energies: 0.10, 0.25 and 0.50 B (1 B $\equiv 10^{51}$ erg). We investigated these small explosion energies based on the recent explosion simulations of ultrastripped SNe by Suwa et al. (2015). They found that ultrastripped SNe explode via the neutrino-driven mechanism and have small explosion energies of the order of 0.1 B.

The results of our nucleosynthesis calculation for the case of $E_{ej} = 0.25$ B is shown in Fig. 3. Table 1 shows the final average abundances in the ejecta for all energies and mass cuts we applied. One of the most important elements determining SN properties is the mass of ^{56}Ni synthesized in the explosion. We find that the ^{56}Ni masses range from 0.034 to 0.021 $M_\odot$ depending on explosion energy and mass cut (Table 1).

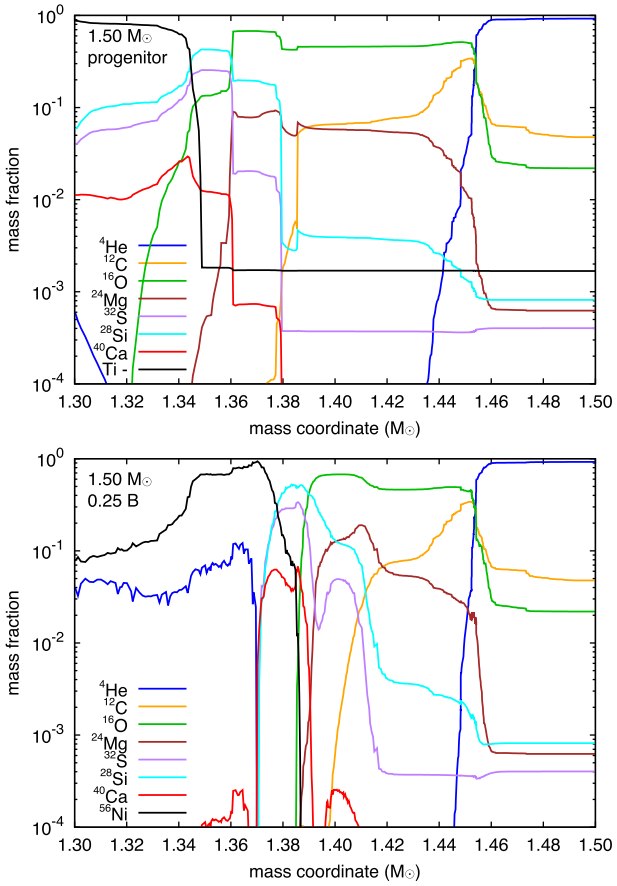

Figure 3. Chemical structure of the 1.50 $M_\odot$ progenitor at iron core collapse (top) and the result of our explosive nucleosynthesis calculation with the explosion energy 0.25 B (bottom). The total abundance above Ti is plotted as a single line in the top panel ('Ti -').

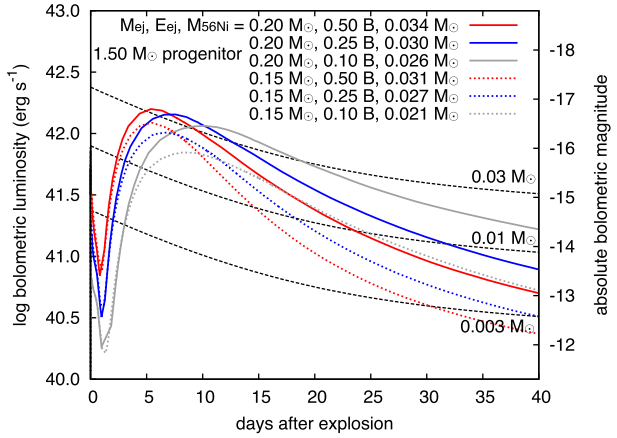

Figure 4. Bolometric LCs of ultrastripped SNe. The thin dashed black lines show the total available energy from the nuclear decay of the indicated ^{56}Ni masses.

3.2 Light curves

Fig. 4 shows the bolometric LCs of ultrastripped SNe obtained in this study. After shock breakout, the bolometric LCs decline in the first 1 d owing to adiabatic cooling of the ejecta. Then, when the heating from ^{56}Ni decay becomes dominant, the bolometric luminosity starts to increase again. The peak luminosity is approximately

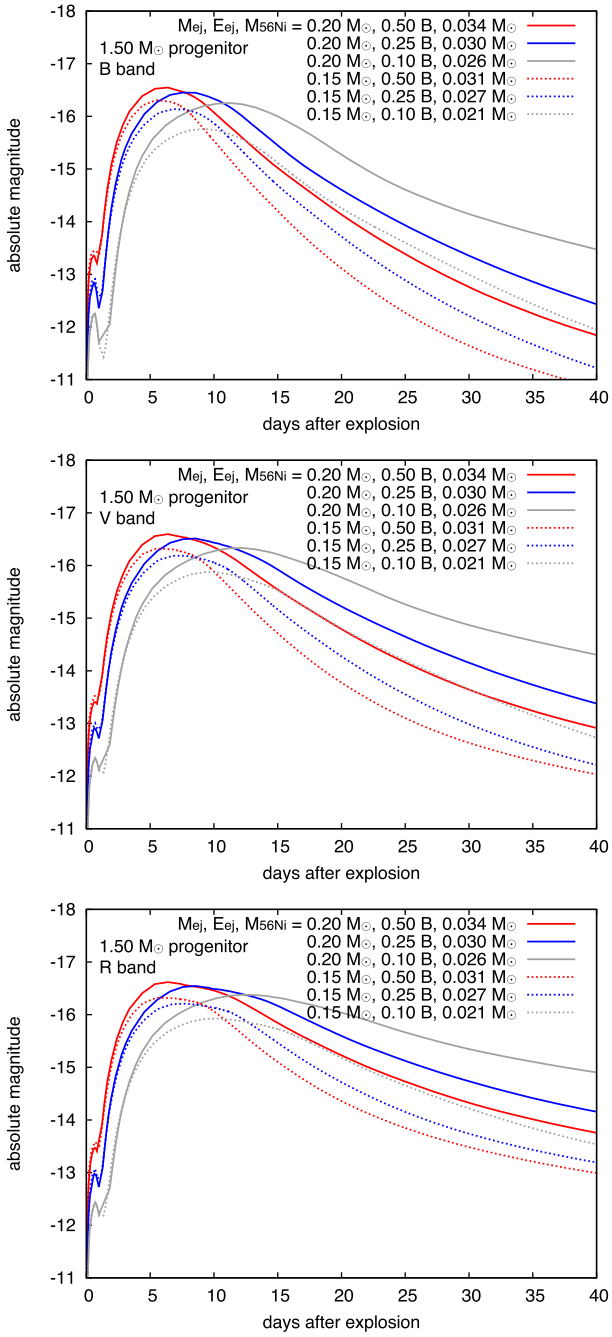

Figure 5. Multicolour LCs for the models shown in Fig. 4.

proportional to the initial ^{56}Ni mass. In most cases, the peak luminosity does not exactly match that expected from a simple estimate based on Arnett (1982); it is larger by up to 50 per cent. The rise time and peak luminosity are consistent with those estimated in Tauris et al. (2015) by using an analytic approach.

Fig. 5 shows multicolour LCs of the same models with several Bessel filters (Bessell 1990). Optical LCs presented in Fig. 5 show some differences from the bolometric LCs. In particular, optical LCs show a first LC peak at times when bolometric LCs monotonically decline. This is a consequence of the cooling of the ejecta, which shifts the spectral peak to longer wavelengths as time goes on. Therefore, LCs in redder bands peak later.

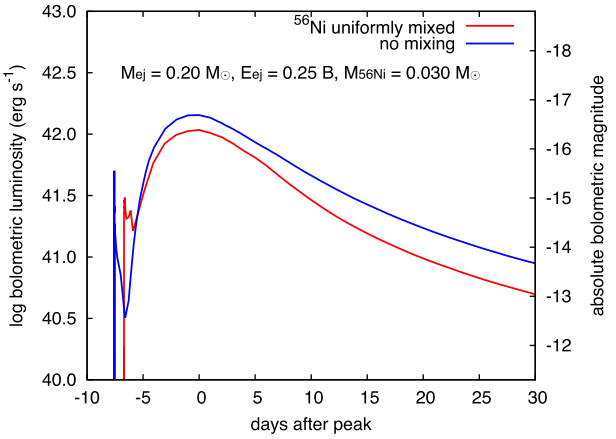

Figure 6. Bolometric LCs with and without ^{56}Ni mixing. Bolometric LCs from the models with $M_{\rm ej} = 0.20\,{\rm M}_\odot$ and $E_{\rm ej} = 0.25\,{\rm B}$ are shown.

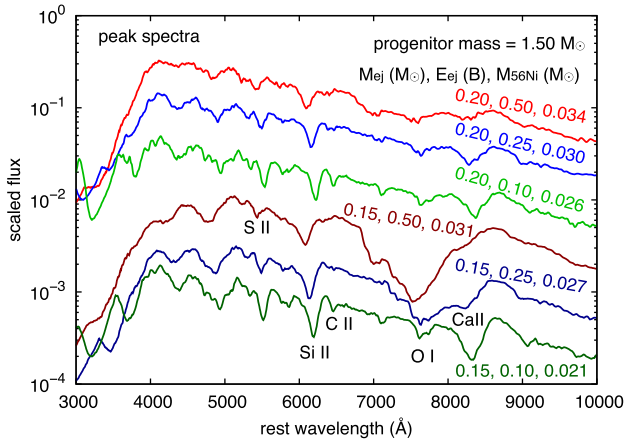

Figure 7. Synthetic spectra at bolometric LC peak for various models. The time of the bolometric LC peak is (from the top spectrum to the bottom) 5.3, 7.5, 10.2, 5.4, 6.8 and 8.2 d.

In the models presented so far, we have used the chemical structure from the explosive nucleosynthesis modelling (cf. Fig. 3) and did not take into account the effect of mixing. To demonstrate the effect of mixing on the LCs, we show an LC in which ^{56}Ni is uniformly mixed in the entire ejecta (Fig. 6). Because of the presence of ^{56}Ni in the outer layers, heating by ^{56}Ni in ejecta is more efficient early on and the rise time becomes shorter in the mixed model. However, at late phases, the gamma-rays in the outer layers are less trapped because of the smaller optical depth. Thus, the luminosity of the mixed model is less than that of the non-mixed model by about 50 per cent. The decline rate after the LC peak is not strongly affected by mixing.

3.3 Spectra

3.3.1 Peak spectra

We present synthetic spectra at maximum light in Fig. 7. We focus on this epoch's spectra because this is when ultrastripped SNe are most likely to be observed. We compare these synthetic spectra with observations in Section 4.2.

Spectral features primarily depend on elemental abundances, photospheric temperature and photospheric velocity. We used the mixed composition in Table 1 for our spectral modelling. Fig. 8

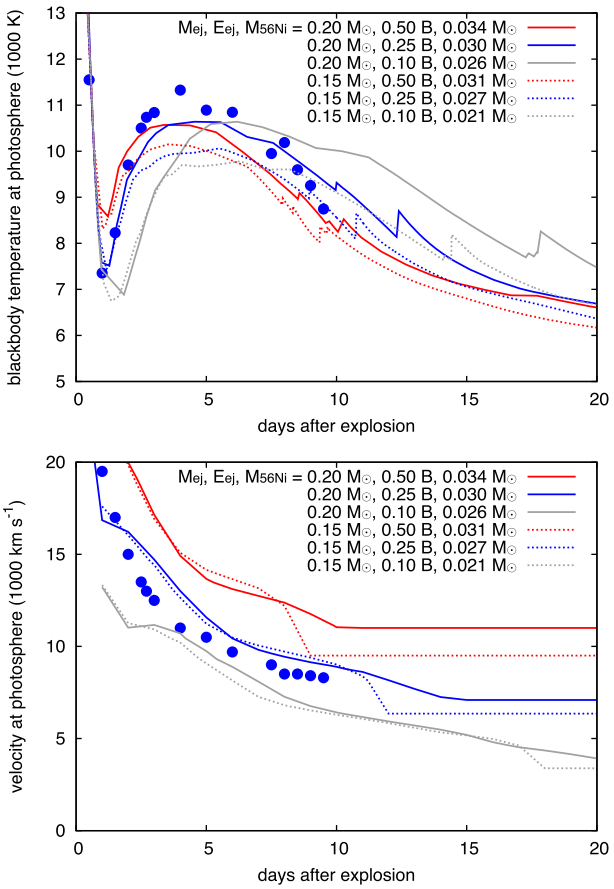

Figure 8. Photospheric temperature and velocity of the models from our STELLA LC calculations (solid and dotted lines). The filled circles indicate the results of the spectral synthesis code using the density structure from STELLA for the $M_{\rm ej} = 0.20\,{\rm M}_\odot$, $E_{\rm ej} = 0.25\,{\rm B}$ model. The synthesized spectra are presented in Fig. 9.

shows the photospheric velocities and temperatures obtained by fitting the blackbody function to the spectral energy distributions obtained from STELLA. The photosphere here is defined as the location where the Rosseland mean optical depth is 2/3. The circles in Fig. 8 represent the values in the converged spectral models of $M_{\rm ej} = 0.20\,{\rm M}_\odot$ and $E_{\rm ej} = 0.25\,{\rm B}$ shown in Fig. 9. The photospheric temperature and velocity from the LC code and the spectral code match within 10 per cent.

Line shifts and broadening in spectra depend on the photospheric velocity. Because velocity is proportional to $(E_{\rm ej}/M_{\rm ej})^{1/2}$, $E_{\rm ej}/M_{\rm ej}$ is a good indicator of these properties. The models with $E_{\rm ej} = 0.25\,{\rm B}$ have $E_{\rm ej}/M_{\rm ej} \simeq 1\,{\rm B}/\,{\rm M}_\odot$, which is similar to typical SNe Ia.

There are several notable features in our synthetic peak spectra. First of all, there are relatively strong Si II features, particularly Si II λ6355. In some models, especially in the spectra with relatively small explosion energy, we can also see the C II λ6582 feature next to Si II λ6355. We can find some S II features between 5000 and 6000 Å. O I λ7774 and Ca II IR triplet around 8000 Å are also seen. The strong Ca feature in the $M_{\rm ej} = 0.15\,{\rm M}_\odot$ and $E_{\rm ej} = 0.50\,{\rm B}$ model is due to Ca ionization as is discussed in the next section.

3.3.2 Temporal evolution

We show the temporal evolution of our synthetic spectra with $M_{\rm ej} = 0.20\,{\rm M}_\odot$ and $E_{\rm ej} = 0.25\,{\rm B}$ in Fig. 9. We first present the

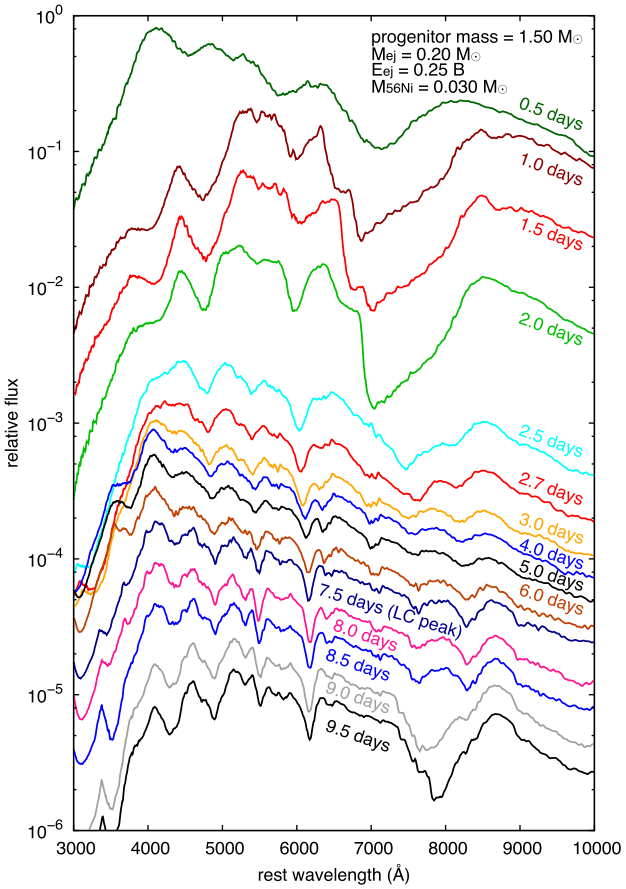

Figure 9. Temporal evolution of spectra for the model with $M_{\rm ej} = 0.20\,{\rm M}_\odot$ and $E_{\rm ej} = 0.25\,{\rm B}$.

spectrum at 0.5 d after the explosion, which is still in the cooling phase after shock breakout (Fig. 4). This epoch roughly corresponds to the time when the optical LCs show the first peak (Fig. 5). The spectra during these very early epochs are similar to those of broad-line Type Ic SNe (SNe Ic-BL) because the photosphere is located in the high-velocity outer layers at that time (cf. Fig. 8).

Up to about 2.5 d after the explosion, a strong Ca absorption is observed between 7000 and 8000 Å. These broad features disappear by the time of LC peak, when the photospheric temperature becomes hot enough to change the Ca ionization level. The broad feature starts to appear again about 9 d after the explosion as the photosphere cools. There is no significant evolution in the spectra around LC peak, and the spectra quickly evolve to become nebular soon thereafter. A further study of the late-time spectra is beyond the scope of this paper.

3.3.3 Helium features

Our progenitor contains about 0.03 $M_\odot$ of helium. This is close to the maximum helium mass that can be hidden without showing significant spectral features in relatively low-mass SNe Ib/Ic (about 0.1 $M_\odot$ of He; Hachinger et al. 2012). It is important to judge whether ultrastripped SNe from our progenitor are expected to be observed as Type Ib or Type Ic. However, the spectral synthesis code we have used so far does not take the non-thermal excitation required for helium excitation into account. Here, we show a spectral model where the effect of the non-thermal excitation is taken into

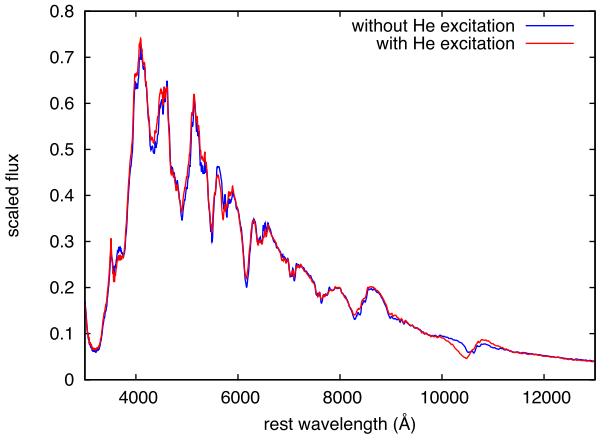

Figure 10. Synthetic spectra with and without non-thermal helium excitation. The original model is the maximum light spectrum of the $M_{\rm ej} = 0.20\,{\rm M}_\odot$, $E_{\rm ej} = 0.25\,{\rm B}$ model with $M_{\rm Ni} = 0.025\,{\rm M}_\odot$, which is also shown in Fig. 7.

account. The spectrum was computed with the spectral synthesis code described in Hachinger et al. (2012).

Fig. 10 shows the spectrum including non-thermal excitation. In the optical range, the spectrum is not strongly affected by non-thermal effects. Helium lines remain invisible except for the intrinsically strong λ10 830 multiplet. Therefore, non-thermal excitation does not seem to cause significant changes to the spectra of ultrastripped SNe.

The fact that He I remains practically invisible in our spectra, while 0.1 $M_\odot$ of helium could be detected in the SN Ib/Ic models of Hachinger et al. (2012), is not only due to the somewhat smaller amount of ^{56}Ni in our models. It can also be traced back to the fact that spectral temperatures are relatively high in our models, such that the non-thermal excitation effects rather result in a high ionization fraction (i.e. dominance of He II) than in a large occupation number within He I excited states possibly generating lines. This is a situation somewhat similar to that of SLSNe (Mazzali et al. 2016).

4 COMPARISON WITH OBSERVATIONS

4.1 Light curves

Fig. 11 shows a comparison between our synthetic LCs and observational data of rapidly evolving SNe. The comparison is shown both in bolometric luminosity and in the *B* band. Overall, our LCs are consistent with faint rapidly evolving SNe with peak luminosity of $\sim 10^{42}\,{\rm erg\,s^{-1}}$ (i.e. ~ -16 mag). Luminous SNe like SN 2002bj require more than 0.1 $M_\odot$ of ^{56}Ni to explain the peak luminosity by ^{56}Ni, which is inconsistent with the small amount of ^{56}Ni ($\sim$0.01 $M_\odot$) we expect in our ultrastripped SNe. Ultrastripped SN LCs are consistent with those of rapidly evolving faint SNe (e.g. SN 2010X, PS1-12bb and SN 2008ha), the so-called Ca-rich gap transients (e.g. PTF10iuv and SN 2005E) and SN 2005ek.

4.2 Spectra

We compare our models with observed near-LC-peak spectra of some rapidly evolving SNe, i.e. SN 2005ek, two Ca-rich gap transients (PTF10iuv and SN 2005E), SN 2010X, SN 2002bj and an SN 2002cx-like SN 2007qd. The observed spectra are taken

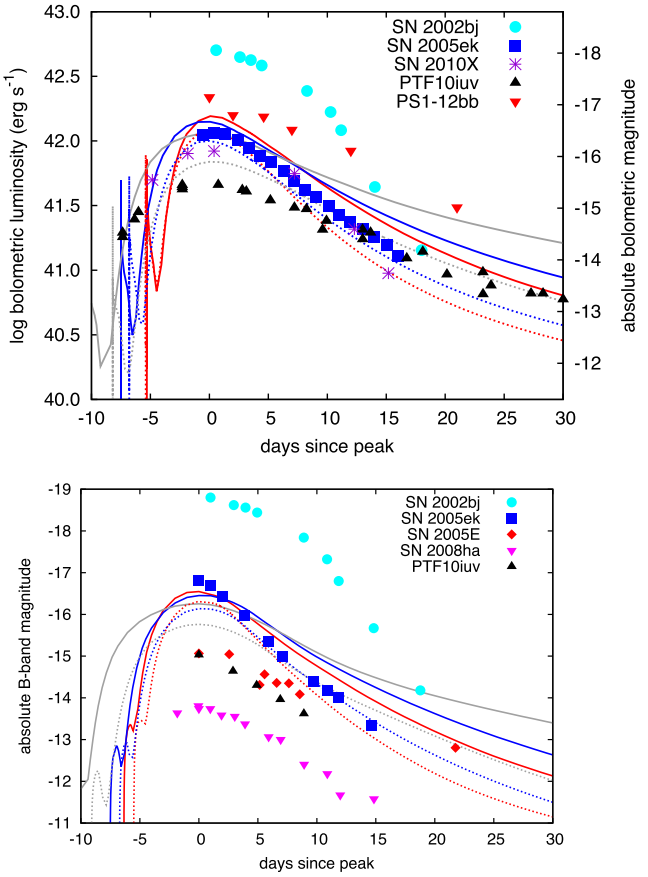

Figure 11. Comparison between our synthetic and observed bolometric (top) and *B*-band (bottom) LCs of rapidly evolving SNe. These are from Drout et al. (2014, PS1-12bb), Kasliwal et al. (2010, SN 2010X), Drout et al. (2013, SN 2005ek), Poznanski et al. (2010, SN 2002bj), Kasliwal et al. (2012, PTF10iuv), Perets et al. (2010, SN 2005E) and Foley et al. (2009, SN 2008ha).

from WISeREP[1] (Yaron & Gal-Yam 2012). We use synthetic spectra of 0.25 B for comparison, as there are no significant differences in spectral features (except for velocity) caused by the difference in the explosion energy in most spectra (Fig. 7). We correct the extinction of observed spectra by using the Galactic extinction law of Cardelli, Clayton & Mathis (1989) assuming $R_V = 3.1$. The redshifts and extinctions applied are, $z = 0.017$ and $E(B-V) = 0.21$ mag for SN 2005ek (Drout et al. 2011), $z = 0.02$ and $E(B-V) = 0$ mag for PTF10iuv (Kasliwal et al. 2012), $z = 0.0090$ and $E(B-V) = 0.098$ mag for SN 2005E (Perets et al. 2010), $z = 0.015$ and $E(B-V) = 0.146$ mag for SN 2010X (Kasliwal et al. 2010), $z = 0.012$ and $E(B-V) = 0$ mag for SN 2002bj (Poznanski et al. 2010) and $z = 0.043$ and $E(B-V) = 0.035$ mag for SN 2007qd (McClelland et al. 2010).

4.2.1 SN 2005ek

SN 2005ek was suggested to be an SN whose progenitor experienced extensive mass stripping by binary interactions (Drout et al. 2013). Its LC was shown to be consistent with our ultrastripped SN model (Tauris et al. 2013), but the spectral properties have not yet been compared.

[1] http://wiserep.weizmann.ac.il

Fig. 12 shows a comparison between synthetic spectra obtained from our ultrastripped SN models and the spectrum of SN 2005ek 1 d before LC peak. Overall, continuum features and velocity shifts of the synthetic spectra match the observed spectrum well. In particular, the characteristic features in the red part of the spectrum of SN 2005ek, i.e. C I λ6582, O I λ7774 and Ca II IR triplet, are all well reproduced by the $M_{\rm ej} = 0.20\,{\rm M}_\odot$ model.

Our models predict stronger Si II features than seen in SN 2005ek. We find that we can obtain a better match by reducing the Si abundance from 0.053 to 0.003 and increasing the O abundance from 0.18 to 0.23 (Fig. 13). The strong Si features in the original ultrastripped SN model may also be due to our assumption of fully mixed ejecta. The average Si abundance used in the spectral modelling is around 0.05, while most of the outer layers have smaller fractions initially (Fig. 3). The smaller abundances may result in weaker Si features especially at early times. Thus, our assumption of full mixing may be too simplistic and SN 2005ek might have had a rather smaller degree of mixing. This may also explain the significant drop in flux below ∼3500 Å in the model: a larger degree of mixing results in more Fe-group elements in the outer layers, leading to more line blocking that suppresses the NUV flux.

4.2.2 Ca-rich gap transients (PTF10iuv and SN 2005E)

Fig. 11 shows the LCs of two Ca-rich gap transients, PTF10iuv and SN 2005E. Their peak luminosity is slightly smaller than that of our ultrastripped SNe, but the time-scales of the LC evolution as well as the LC decline rates are similar. Efficient mixing in the ejecta may make the luminosity of our models slightly lower (Fig. 6), which motivates us to investigate their spectra.

Fig. 14 shows a spectral comparison near peak luminosity. The spectral features including velocity shifts of PTF10iuv (top panels of Fig. 14) match our models well. Prominent features in PTF10iuv such as Si II λ6347, O I λ7772 and Ca II λ8542 are also well reproduced. We find relatively strong Si and Ca lines from our core-collapse progenitors because of the small values of the explosion energy and the progenitor mass. The overall colour of PTF10iuv is consistent with our model. In summary, the LC and spectral properties of PTF10iuv are overall consistent with our ultrastripped SN models.

On the other hand, our ultrastripped SN spectral models are not consistent with the spectral features of the other Ca-rich gap transient, SN 2005E, very well, as shown in the bottom panels of Fig. 14. This indicates that there may be several kinds of progenitors for Ca-rich gap transients, of which some could be related to ultrastripped SNe.

Ca-rich gap transients are typically found in remote locations from the centre of their host galaxies (Kasliwal et al. 2012; Lyman et al. 2014, 2016b; Foley 2015). For example, PTF10iuv was 40 kpc away from the closest host galaxy candidate (Kasliwal et al. 2012). This fact is used to relate Ca-rich gap transients to explosive events related to white dwarfs. However, Ca-rich transients are also found in the intergalactic space of merging galaxies (e.g. Foley 2015), where star formation is likely to take place (e.g. Mullan et al. 2011). Some massive stars are also known to exist very far from apparent star-forming regions (e.g. Smith, Andrews & Mauerhan 2016). It is also interesting to note that white dwarf mergers may actually end up as core-collapse SNe and could lead to SNe with similar properties to our ultrastripped SNe (e.g. Nomoto & Iben 1985; Schwab, Quataert & Kasen 2016).

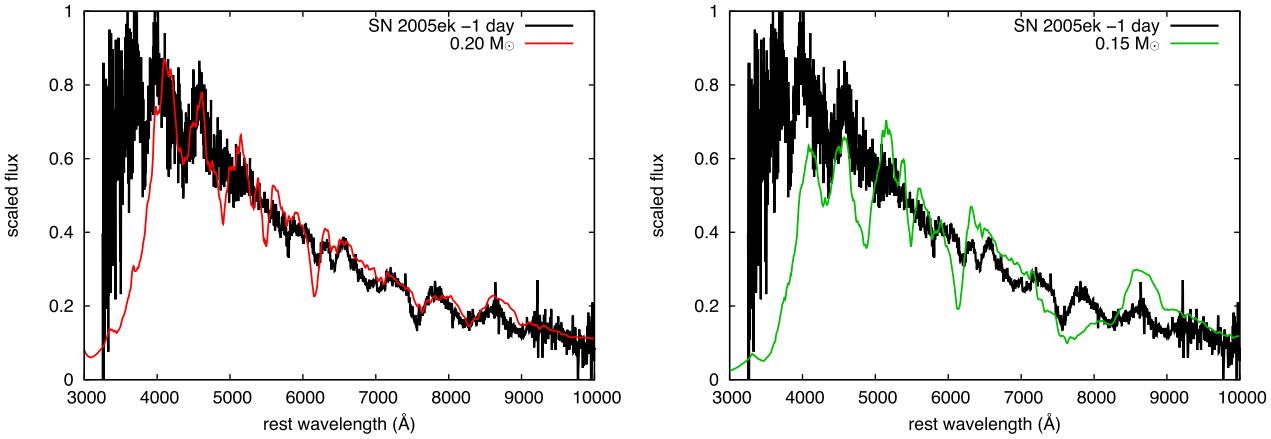

Figure 12. Comparison between our synthetic spectra and the observed spectrum of SN 2005ek 1 d before LC peak from Drout et al. (2013).

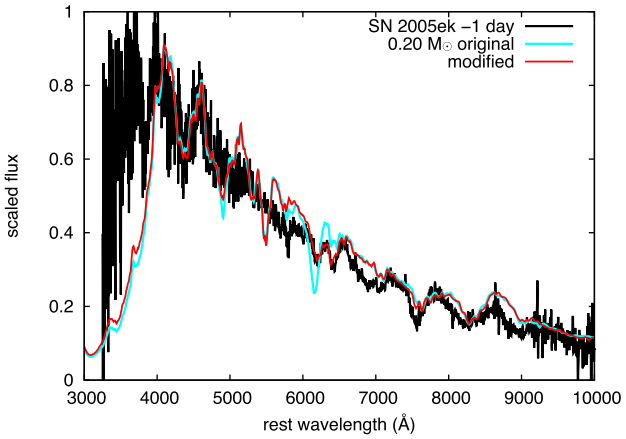

Figure 13. Synthetic spectrum for the $M_{\rm ej} = 0.20\,{\rm M}_{\odot}$ and $E_{\rm ej} = 0.25$ B model, where the Si abundance is artificially reduced and the O abundance is artificially increased. The model provides a better match than the original one.

As we suggest here, Ca-rich gap transients can have different origin. Those found far from any host galaxy may be unrelated to ultra-stripped SNe. The faint nature of ultrastripped SNe may also prevent them from being found in bright star-forming regions such as in galactic discs.

4.2.3 SN 2010X

SN 2010X was a rapidly evolving Type Ib SN. Its ejecta mass was estimated to be $\sim$0.16 $M_{\odot}$ and its ^{56}Ni mass to be $\sim$0.02 $M_{\odot}$ (Kasliwal et al. 2010). These properties, as well as the LC evolution are similar to those of our ultrastripped SNe (Fig. 11). SN 2010X had spectral characteristics similar to SN 2002bj, which we discuss in the next section, but it was much fainter.

We compare our spectra with that of SN 2010X near LC peak in Fig. 15. Overall spectral features match well, especially the model with $M_{\rm ej} = 0.15\,{\rm M}_{\odot}$. The Si II λ6355 is predicted to be slightly stronger, but a small reduction of the Si abundance or a slightly smaller degree of mixing could reduce the strength of this line as was discussed for SN 2005ek. Therefore, SN 2010X may also be related to ultrastripped SNe.

4.2.4 SN 2002bj

SN 2002bj was one of the first rapidly evolving SNe to be reported (Poznanski et al. 2010). If SN 2002bj was powered by ^{56}Ni, the amount of ^{56}Ni required to explain its peak luminosity is 0.15–0.25 $M_{\odot}$ (Poznanski et al. 2010, see also Fig. 11). The amount of ^{56}Ni required is much larger than what we expect from ultrastripped SNe, and the ^{56}Ni mass alone is comparable to the total ejecta mass expected from ultrastripped SNe. This suggests that SN 2002bj is unlikely to be related to ultrastripped SNe. None the less, we show the comparison between our synthetic spectra and that of SN 2002bj. As expected, the match is not very good (Fig. 16).

4.2.5 SN 2002cx-like (Type Iax) SNe

SN 2002cx-like SNe, which are often referred as Type Iax SNe, are a peculiar type of SN Ia with fainter peak luminosity. Their origin is still under discussion (e.g. Foley et al. 2016). Although many of them have peak magnitudes brighter than -17 mag (see Foley et al. 2016 for a summary) and are thus too bright to be ultrastripped SNe, some of them do have fainter peak luminosity (e.g. McClelland et al. 2010; Stritzinger et al. 2014). We take one faint SN 2002cx-like SN, SN 2007qd (McClelland et al. 2010), which is in the expected peak luminosity range for ultrastripped SNe, and compare its spectrum at the peak luminosity with our synthetic spectra.

Fig. 17 shows the comparison. SN 2002cx-like SNe have much lower velocities than our synthetic ultrastripped SN spectra. A low photospheric velocity is a commonly observed feature of faint SN 2002cx-like SNe. Our model with the smallest explosion energy (0.10 B) may have a photospheric velocity similar to that of some SN 2002cx-like SNe (Fig. 8), but it still seems to fail to reproduce crowded, unblended line features. In addition, the spectra of ultrastripped SNe evolve quickly to the nebular regime, while the spectra of SN 2002cx-like SNe do not (e.g. Sahu et al. 2008; Foley et al. 2016).

4.3 Summary

Table 2 summarizes the results of the comparison between our ultrastripped SN models and possible observational counterparts. We find that SN 2005ek, PTF10iuv (Ca-rich gap transient) and SN 2010X match our synthetic ultrastripped SN LCs and spectra.

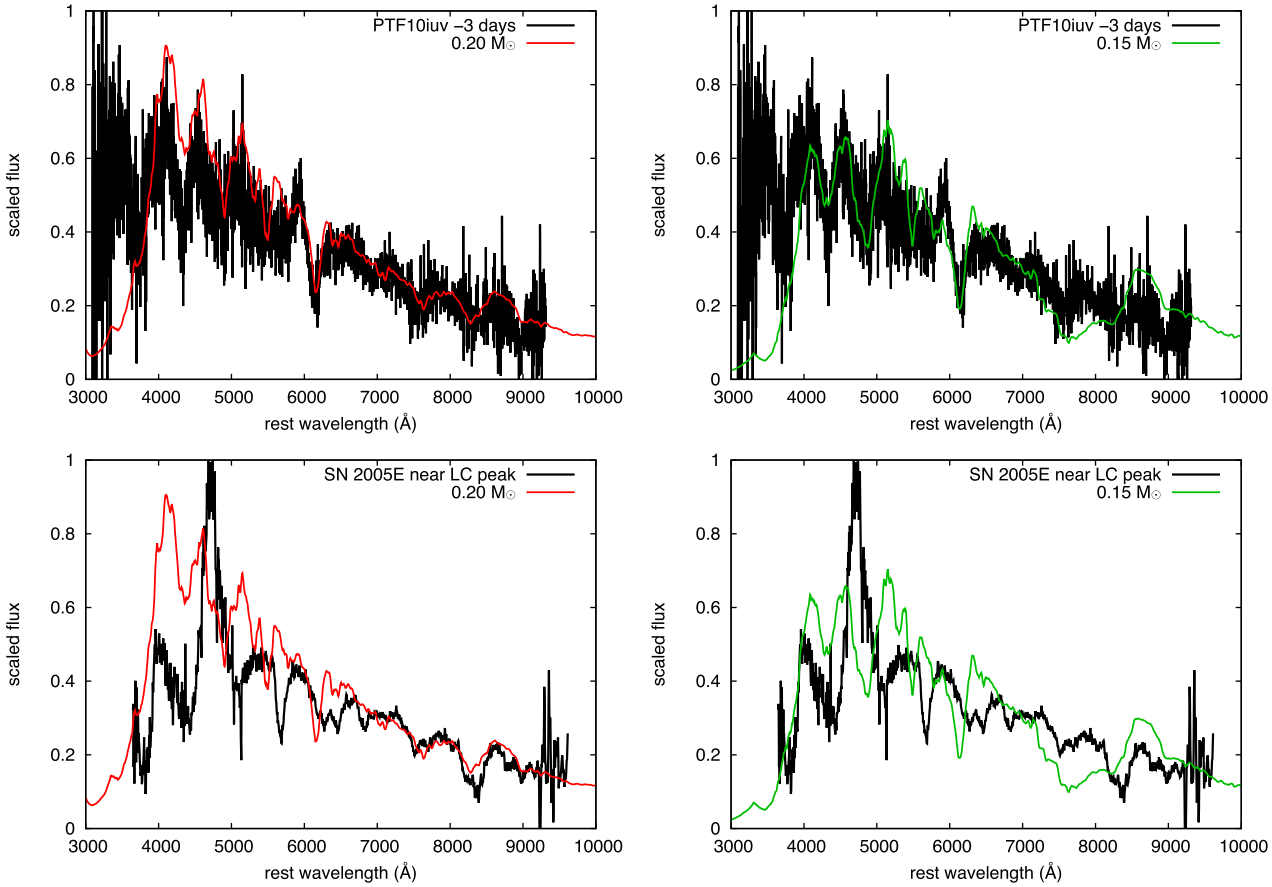

Figure 14. Comparison between our synthetic spectra and the observed near-maximum spectra of the Ca-rich gap transients PTF10iuv (Kasliwal et al. 2012) and SN 2005E (Perets et al. 2010).

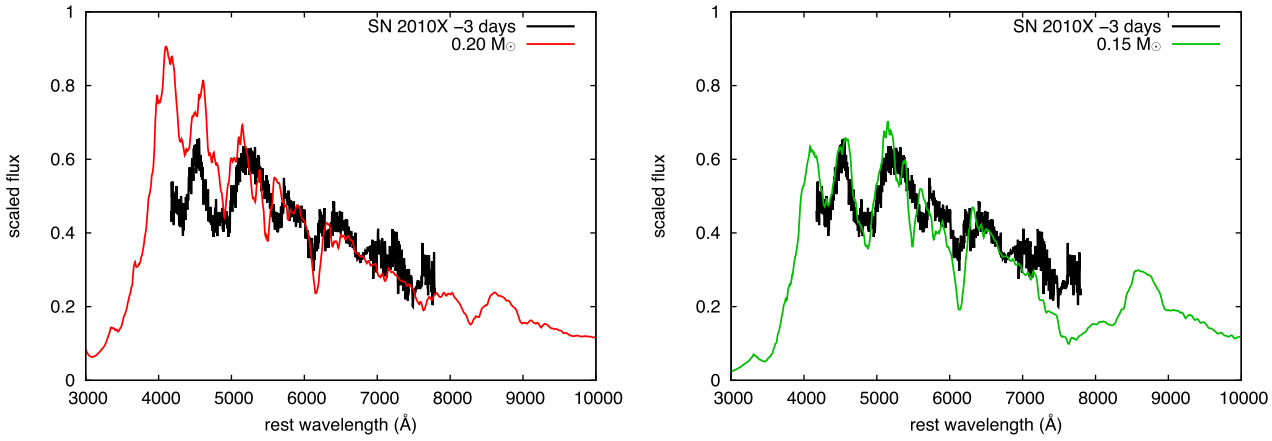

Figure 15. Comparison between our synthetic spectra and the spectrum of SN 2010X (Kasliwal et al. 2010) near LC peak.

5 DISCUSSION

5.1 Diversity

We have investigated the observational properties of an ultrastripped SN explosion from a progenitor with a mass of 1.50 $M_\odot$. Depending on the initial binary parameters and the helium ZAMS mass of the progenitor, the final total mass and core mass vary considerably (Tauris et al. 2015). However, recent numerical simulations of explosions of ultrastripped core-collapse SNe find that the explosion energy and the synthesized ^{56}Ni mass do not change significantly among progenitors of different core masses (Suwa et al. 2015). Thus, the explosion energy and ^{56}Ni mass values investigated in this paper are likely to remain similar even in different ultrastripped SN progenitors. The low spread in the ^{56}Ni masses found in our models suggests that the peak luminosity should be roughly similar in all ultrastripped SNe, although the LC rise time can vary depending on the ejecta mass (Tauris et al. 2015). In our one-dimensional model, the ^{56}Ni mass ejected depends on the mass cut, but Suwa et al. (2015) obtained similar ^{56}Ni masses in their multidimensional

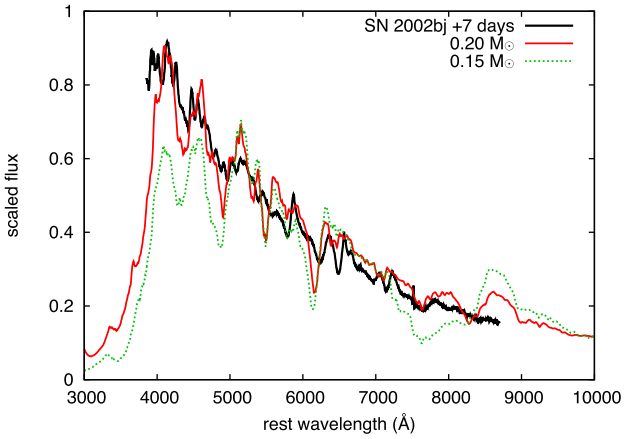

Figure 16. Comparison between our synthetic spectra at maximum and the earliest observed spectrum of SN 2002bj (Poznanski et al. 2010).

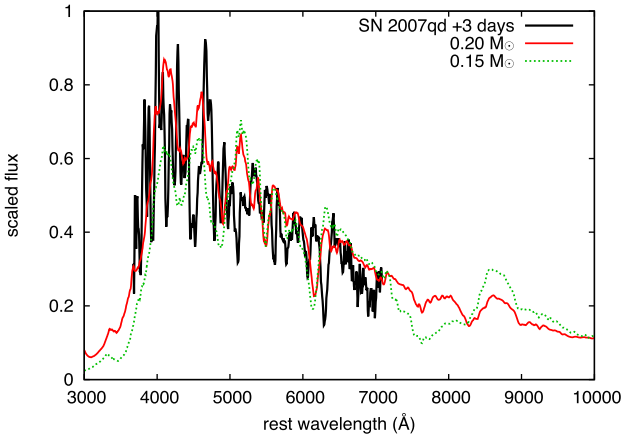

Figure 17. Comparison between our synthetic spectra at maximum and the observed spectrum of the SN 2002cx-like SN 2007qd near maximum (McClelland et al. 2010).

explosion simulations. Thus, the spectral signatures we find in this study for a particular progenitor model are likely to be generic for ultrastripped SNe.

A possible major source of diversity in ultrastripped SN properties that may be caused by differences in their progenitors is their SN spectral type, which is determined by the ejected helium mass. In the progenitor model we used in this study, there are 0.03 $M_\odot$ of helium in an ejected mass of 0.15–0.20 $M_\odot$. Although helium features are not expected to be observed significantly in our model and we expect the explosion to be an SN Ic (Section 3.3.3), the helium mass as well as the ejecta mass can change depending on the initial binary configurations (Tauris et al. 2015). Many progenitors are expected to have a helium mass above the critical helium mass (~0.1 $M_\odot$; Hachinger et al. 2012) required to observe optical helium features (Tauris et al. 2015), and thus may be observed as SNe Ib like SN 2010X.

To summarize, the expected luminosity range of ultrastripped SNe is similar to that obtained with the model used in this paper. The diversity in SN ejecta masses caused by different progenitor systems could lead to diversity in the rise times of ultrastripped SNe. We indicate the expected location of ultrastripped SNe in the phase diagram of transients (e.g. Kulkarni 2012) in Fig. 18. It is likely that there is a smooth transition between ultrastripped SNe and stripped-envelope SNe. The classical Type Ic SN 1994I, which had an ejecta mass of only 1 $M_\odot$ (e.g. Iwamoto et al. 1994; Sauer et al. 2006) may be an example of an SN Ic located between typical stripped-envelope SNe and ultrastripped SNe. Also, the low-mass Type Ic SN 2007gr (Hunter et al. 2009; Mazzali et al. 2010) may be an even more extreme case.

Table 2. Ultrastripped SN candidates. An '√' or an 'x' indicate whether or not the SN properties match those expected of ultrastripped SNe.

SN	LC	Velocity	Si	Ca
SN 2005ek	√	√	√	√
PTF10iuv (Ca-rich gap)	√	√	√	√
SN 2005E (Ca-rich gap)	√	x	x	√
SN 2010X	√	√	√	√
SN 2002bj	x	x	x	x
SN 2007qd (02cx-like)	√	x	√	?

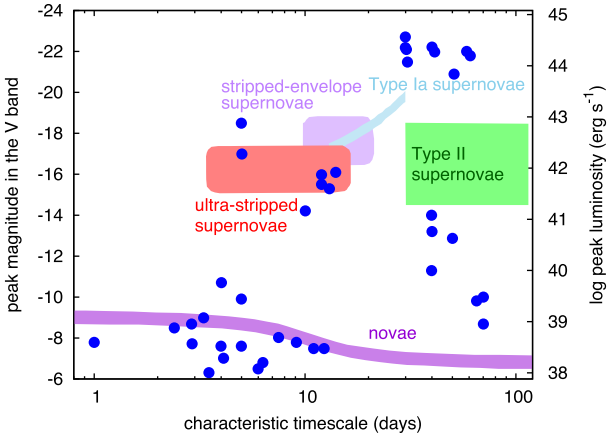

Figure 18. Characteristics of ultrastripped SNe in the phase-space diagram of optical transients from Kulkarni (2012).

5.2 Event rates

Based on our spectral analysis, we have shown that SN 2005ek and some of the Ca-rich gap transients, as well as SN 2010X, might be related to ultrastripped SNe. The event rate of rapidly evolving SNe including SN 2005ek, SN 2010X and SN 2002bj are estimated to be at least 1–3 per cent of SNe Ia (Drout et al. 2013). The total event rate of the Ca-rich gap transients is estimated to be at least a few per cent of SNe Ia (Perets et al. 2010; Kasliwal et al. 2012). Given that a part of the transients included to estimate the two event rates actually correspond to ultrastripped SNe, we can roughly estimate that the event rate for the ultrastripped SNe based on SN observations is at least a few per cent of SNe Ia. Because the volumetric rates of SNe Ia and SNe Ib/Ic are similar (e.g. Li et al. 2011), ultrastripped SN rates are presumed to be at least a few per cent of SNe Ib/Ic. This rate corresponds to roughly 1 per cent of all core-collapse SNe including SNe II (Li et al. 2011) and matches the rough event rate estimate by Tauris et al. (2013, 0.1–1 per cent of core-collapse SNe). Further observational and theoretical studies to better estimate the event rate of ultrastripped SNe are encouraged for their better comparison.

5.3 Synergy with GW astronomy

Because ultrastripped SNe are presumed to lead to double-NS systems, but not all double-NS systems merge within a Hubble time, the observed rate of ultrastripped SNe is expected to be larger than

the rate of double-NS mergers. Furthermore, ultrastripped SNe may also originate in binary systems with a white dwarf or a black hole accretor (Tauris et al. 2013). After the recent success in detecting GW signals from merging compact objects by advanced LIGO (Abbott et al. 2016a), it is expected that GW from merging double-NS systems will be detected in the near future, with advanced LIGO or other detectors like advanced VIRGO and KAGRA. Thus, it will soon be possible to obtain NS merger rate constraints from GW observations. This should place a lower limit to the rate of ultra-stripped SNe. Comparing the rates of ultrastripped SNe and NS mergers, we will be able to test whether the ultrastripped SN channel is actually the major path to form double-NS systems, and thus to constrain binary stellar evolution using GW.

The current constraints on the NS merger rate from LIGO is less than $12\,600\,\mathrm{Gpc^{-3}\,yr^{-1}}$ (Abbott et al. 2016b). Assuming the Galactic core-collapse SN rate of $\sim$0.01 $\mathrm{yr^{-1}}$ and ultrastripped SN fraction of 0.1–1 per cent in core-collapse SNe, we obtain an expected Galactic ultrastripped SN rate of $\sim10^{-5}$–$10^{-4}\,\mathrm{yr^{-1}}$. If we adopt the Milky Way equivalent galaxy density of $0.01\,\mathrm{Mpc^{-3}}$ (Kopparapu et al. 2008), we expect an ultrastripped SN rate of $\sim$100–$1000\,\mathrm{Gpc^{-3}\,yr^{-1}}$. This is significantly lower than the current upper limit on the NS–NS merger rate from LIGO.

Finally, it should be noted that the distribution of eccentricities in current observations of NS–NS binaries (Martinez et al. 2015; Lazarus et al. 2016) supports the idea that ultrastripped SNe are indeed the progenitors of the second SN in these systems, and that they often (but not always) result in small kicks. Out of 12 NS–NS systems, 9 have an eccentricity of less than 0.3. Moreover, even relatively small NS kicks of $50\,\mathrm{km\,s^{-1}}$ can result in post-SN eccentricities of more than 0.5, depending on the orbital period (Tauris et al., in preparation).

5.4 Observations of ultrastripped SN progenitors

While it has been argued that the descendants of ultrastripped SNe are often close pairs of NSs in binaries, it is much more difficult to find direct observational evidence for the progenitors of ultra-stripped SNe. Arguably, a fraction of high-mass X-ray binaries currently containing an NS and an OB-star will eventually evolve into double NS systems. Others will merge or become disrupted in the process. However, in between these two stages, the immediate progenitors of ultrastripped stars would be found either as post-common-envelope naked helium stars (Wolf–Rayet stars) or in an X-ray binary during the subsequent so-called Case BB Roche lobe overflow. However, these phases are short lasting (especially the latter that is typically $<10^5$ yr; Tauris et al. 2015) and thus chances of detecting these systems are small, even though the helium star is rather luminous ($>10^4\,\mathrm{L_\odot}$). One possible related observed system is Cygnus X-3 that is a close binary system with an NS or BH and a Wolf–Rayet star, but the mass of the Wolf–Rayet star (about 10 $\mathrm{M_\odot}$; Zdziarski, Mikołajewska & Belczyński 2013) is too high to correspond to an ultrastripped SN progenitor.

6 CONCLUSIONS

We have presented synthetic LCs and spectral properties of ultra-stripped SNe. We evolved the ultrastripped SN progenitor presented previously (Tauris et al. 2013) until core collapse, calculated its explosive nucleosynthesis, and then synthesized LCs and spectra. Our ultrastripped SNe have explosion energies of 1–5 $\times$ 10^{50} erg and ejecta masses of $\sim$0.1 $\mathrm{M_\odot}$. Explosive nucleosynthesis calculations show that they produce about $0.03\,\mathrm{M_\odot}$ of ^{56}Ni. We also found that ultrastripped SNe have rise times of 5–10 d and their peak luminosity is $\sim-$ 16 mag or $10^{42}\,\mathrm{erg\,s^{-1}}$.

Several types of transients have been found that have rise times and peak luminosities similar to those expected for ultrastripped SNe. They show diverse spectral properties. We compared our synthetic spectra with those of rapidly evolving transients showing LCs similar to those of our synthetic ultrastripped SN LCs, and found that the spectra of SN 2005ek, some of so-called Ca-rich gap transients, and SN 2010X match reasonably well our synthetic ultrastripped SN spectra. Not all Ca-rich gap transients have similar properties to our ultrastripped SNe, indicating that this group of transients may include events with different origin. For example, the spectra of PTF10iuv are consistent with our ultrastripped SN spectra, while those of SN 2005E are not. If all the transients above mentioned are actually from ultrastripped SNe, the event rate of ultrastripped SNe would be about 1 per cent of all stripped-envelope SNe.

It has been suggested that ultrastripped SNe may be a major evolutionary path to form double-NS systems that could merge within a Hubble time and that double-NS systems left by ultra-stripped SNe may dominate the population of merging double-NS systems that is expected to be observed by GW observatories (Tauris et al. 2013, 2015). If this is true, we expect the NS merger rate to be comparable to or somewhat smaller than that of ultra-stripped SNe.

ACKNOWLEDGEMENTS

TJM thanks Yudai Suwa and Markus Kromer for helpful discussions. TJM is supported by Japan Society for the Promotion of Science Postdoctoral Fellowships for Research Abroad (26·51) and by the Grant-in-Aid for Research Activity Start-up of the Japan Society for the Promotion of Science (16H07413). The work of SIB on development of STELLA code is supported by Russian Science Foundation grant 14-12-00203. The work has also been supported by a Humboldt Research Award to PhP at the University of Bonn. Numerical computations were partially carried out on Cray XC30 and PC cluster at Center for Computational Astrophysics, National Astronomical Observatory of Japan. The numerical calculations were also partly carried out on Cray XC40 at Yukawa Institute for Theoretical Physics in Kyoto University. We made use of the Weizmann interactive SN data repository – http://wiserep.weizmann.ac.il. This research has made use of the NASA/IPAC Extragalactic Database (NED) that is operated by the Jet Propulsion Laboratory, California Institute of Technology, under contract with the National Aeronautics and Space Administration.

REFERENCES

Abadie J. et al., 2010, Class. Quantum Gravity, 27, 173001
Abbott B. P. et al., 2016a, Phys. Rev. Lett., 116, 061102
Abbott B. P. et al., 2016b, ApJ, 832, L21
Argast D., Samland M., Thielemann F.-K., Qian Y.-Z., 2004, A&A, 416, 997
Arnett W. D., 1982, ApJ, 253, 785
Baklanov P. V., Blinnikov S. I., Pavlyuk N. N., 2005, Astron. Lett., 31, 429
Barnes J., Kasen D., 2013, ApJ, 775, 18
Benvenuto O. G., Bersten M. C., Nomoto K., 2013, ApJ, 762, 74
Berry C. P. L. et al., 2015, ApJ, 804, 114
Bersten M. C. et al., 2012, ApJ, 757, 31
Bersten M. C. et al., 2014, AJ, 148, 68
Bessell M. S., 1990, Publ. Astron. Soc. Pac., 102, 1181
Blinnikov S. I., Bartunov O. S., 1993, A&A, 273, 106
Blinnikov S., Sorokina E., 2004, Ap&SS, 290, 13

Blinnikov S. I., Novikov I. D., Perevodchikova T. V., Polnarev A. G., 1984, Sov. Astron. Lett., 10, 177
Blinnikov S. I., Eastman R., Bartunov O. S., Popolitov V. A., Woosley S. E., 1998, ApJ, 496, 454
Blinnikov S. I., Röpke F. K., Sorokina E. I., Gieseler M., Reinecke M., Travaglio C., Hillebrandt W., Stritzinger M., 2006, A&A, 453, 229
Brandt N., Podsiadlowski P., 1995, MNRAS, 274, 461
Brott I. et al., 2011, A&A, 530, A115
Cardelli J. A., Clayton G. C., Mathis J. S., 1989, ApJ, 345, 245
Colella P., Woodward P. R., 1984, J. Comput. Phys., 54, 174
Dessart L., Hillier D. J., 2015, MNRAS, 447, 1370
Dessart L., Hillier D. J., Woosley S., Livne E., Waldman R., Yoon S.-C., Langer N., 2015, MNRAS, 453, 2189
Drout M. R. et al., 2011, ApJ, 741, 97
Drout M. R. et al., 2013, ApJ, 774, 58
Drout M. R. et al., 2014, ApJ, 794, 23
Eldridge J. J., Maund J. R., 2016, MNRAS, 461, L117
Eldridge J. J., Izzard R. G., Tout C. A., 2008, MNRAS, 384, 1109
Eldridge J. J., Langer N., Tout C. A., 2011, MNRAS, 414, 3501
Eldridge J. J., Fraser M., Smartt S. J., Maund J. R., Crockett R. M., 2013, MNRAS, 436, 774
Eldridge J. J., Fraser M., Maund J. R., Smartt S. J., 2015, MNRAS, 446, 2689
Ensman L. M., Woosley S. E., 1988, ApJ, 333, 754
Ergon M. et al., 2015, A&A, 580, A142
Foley R. J., 2015, MNRAS, 452, 2463
Foley R. J. et al., 2009, AJ, 138, 376
Foley R. J. et al., 2013, ApJ, 767, 57
Foley R. J., Jha S. W., Pan Y.-C., Zheng W. K., Bildsten L., Filippenko A. V., Kasen D., 2016, MNRAS, 461, 433
Fremling C. et al., 2014, A&A, 565, A114
Hachinger S., Mazzali P. A., Taubenberger S., Hillebrandt W., Nomoto K., Sauer D. N., 2012, MNRAS, 422, 70
Hachisu I., Matsuda T., Nomoto K., Shigeyama T., 1991, ApJ, 368, L27
Heger A., Langer N., Woosley S. E., 2000, ApJ, 528, 368
Hirai Y., Ishimaru Y., Saitoh T. R., Fujii M. S., Hidaka J., Kajino T., 2015, ApJ, 814, 41
Hunter D. J. et al., 2009, A&A, 508, 371
Inserra C. et al., 2015, ApJ, 799, L2
Iwamoto K., Nomoto K., Höflich P., Yamaoka H., Kumagai S., Shigeyama T., 1994, ApJ, 437, L115
Izzard R. G., Ramirez-Ruiz E., Tout C. A., 2004, MNRAS, 348, 1215
Jerkstrand A., Ergon M., Smartt S. J., Fransson C., Sollerman J., Taubenberger S., Bersten M., Spyromilio J., 2015, A&A, 573, A12
Jones S. et al., 2013, ApJ, 772, 150
Kashiyama K., Quataert E., 2015, MNRAS, 451, 2656
Kasliwal M. M. et al., 2010, ApJ, 723, L98
Kasliwal M. M. et al., 2012, ApJ, 755, 161
Kawabata K. S. et al., 2010, Nature, 465, 326
Kitaura F. S., Janka H.-T., Hillebrandt W., 2006, A&A, 450, 345
Kleiser I. K. W., Kasen D., 2014, MNRAS, 438, 318
Kopparapu R. K., Hanna C., Kalogera V., O'Shaughnessy R., González G., Brady P. R., Fairhurst S., 2008, ApJ, 675, 1459
Kulkarni S. R., 2012, in Griffin E., Hanisch R., Seaman R., eds, Proc. IAU Symp. 285, New Horizons in Time-Domain Astronomy. Cambridge Univ. Press, Cambridge, p. 55
Langer N., 2012, ARA&A, 50, 107
Lazarus P. et al., 2016, ApJ, 831, 150
Li W. et al., 2011, MNRAS, 412, 1441
Lucy L. B., 1991, ApJ, 383, 308
Lucy L. B., 1999, A&A, 345, 211
Lyman J. D., Levan A. J., Church R. P., Davies M. B., Tanvir N. R., 2014, MNRAS, 444, 2157
Lyman J. D., Bersier D., James P. A., Mazzali P. A., Eldridge J. J., Fraser M., Pian E., 2016a, MNRAS, 457, 328
Lyman J. D., Levan A. J., James P. A., Angus C. R., Church R. P., Davies M. B., Tanvir N. R., 2016b, MNRAS, 458, 1768
McClelland C. M. et al., 2010, ApJ, 720, 704
Marchant P., Langer N., Podsiadlowski P., Tauris T. M., Moriya T. J., 2016, A&A, 588, A50
Martinez J. G. et al., 2015, ApJ, 812, 143
Mazzali P. A., 2000, A&A, 363, 705
Mazzali P. A., Lucy L. B., 1993, A&A, 279, 447
Mazzali P. A., Lucy L. B., 1998, MNRAS, 295, 428
Mazzali P. A., Lucy L. B., Butler K., 1992, A&A, 258, 399
Mazzali P. A., Lucy L. B., Danziger I. J., Gouiffes C., Cappellaro E., Turatto M., 1993, A&A, 269, 423
Mazzali P. A., Iwamoto K., Nomoto K., 2000, ApJ, 545, 407
Mazzali P. A., Nomoto K., Patat F., Maeda K., 2001, ApJ, 559, 1047
Mazzali P. A., Maurer I., Valenti S., Kotak R., Hunter D., 2010, MNRAS, 408, 87
Mazzali P. A., Sullivan M., Pian E., Greiner J., Kann D. A., 2016, MNRAS, 458, 3455
Metzger B. D. et al., 2010, MNRAS, 406, 2650
Modjaz M., Liu Y. Q., Bianco F. B., Graur O., 2015, ApJ, 832, 108
Moriya T. J., Eldridge J. J., 2016, MNRAS, 461, 2155
Moriya T. J., Maeda K., 2016, ApJ, 824, 100
Moriya T., Tominaga N., Tanaka M., Nomoto K., Sauer D. N., Mazzali P. A., Maeda K., Suzuki T., 2010, ApJ, 719, 1445
Mullan B. et al., 2011, ApJ, 731, 93
Nakamura T., Umeda H., Iwamoto K., Nomoto K., Hashimoto M.-a., Hix W. R., Thielemann F.-K., 2001, ApJ, 555, 880
Narayan R., Paczynski B., Piran T., 1992, ApJ, 395, L83
Nomoto K., Iben I., Jr, 1985, ApJ, 297, 531
Nomoto K., Yamaoka H., Pols O. R., van den Heuvel E. P. J., Iwamoto K., Kumagai S., Shigeyama T., 1994, Nature, 371, 227
Nomoto K. I., Iwamoto K., Suzuki T., 1995, Phys. Rep., 256, 173
Ofek E. O. et al., 2010, ApJ, 724, 1396
Paczynski B., 1986, ApJ, 308, L43
Paxton B., Bildsten L., Dotter A., Herwig F., Lesaffre P., Timmes F., 2011, ApJS, 192, 3
Paxton B. et al., 2013, ApJS, 208, 4
Paxton B. et al., 2015, ApJS, 220, 15
Perets H. B. et al., 2010, Nature, 465, 322
Podsiadlowski P., Joss P. C., Hsu J. J. L., 1992, ApJ, 391, 246
Podsiadlowski P., Mazzali P. A., Nomoto K., Lazzati D., Cappellaro E., 2004a, ApJ, 607, L17
Podsiadlowski P., Langer N., Poelarends A. J. T., Rappaport S., Heger A., Pfahl E., 2004b, ApJ, 612, 1044
Poznanski D. et al., 2010, Science, 327, 58
Prentice S. J. et al., 2016, MNRAS, 458, 2973
Rosswog S., Liebendörfer M., Thielemann F.-K., Davies M. B., Benz W., Piran T., 1999, A&A, 341, 499
Sahu D. K. et al., 2008, ApJ, 680, 580
Sauer D. N., Mazzali P. A., Deng J., Valenti S., Nomoto K., Filippenko A. V., 2006, MNRAS, 369, 1939
Schwab J., Quataert E., Bildsten L., 2015, MNRAS, 453, 1910
Schwab J., Quataert E., Kasen D., 2016, MNRAS, 463, 3461
Shen K. J., Kasen D., Weinberg N. N., Bildsten L., Scannapieco E., 2010, ApJ, 715, 767
Shigeyama T., Suzuki T., Kumagai S., Nomoto K., Saio H., Yamaoka H., 1994, ApJ, 420, 341
Smith N., Li W., Filippenko A. V., Chornock R., 2011, MNRAS, 412, 1522
Smith N., Andrews J. E., Mauerhan J. C., 2016, MNRAS, 463, 2904
Sorokina E., Blinnikov S., Nomoto K., Quimby R., Tolstov A., 2015, ApJ, 829, 17
Stritzinger M. D. et al., 2014, A&A, 561, A146
Suwa Y., Yoshida T., Shibata M., Umeda H., Takahashi K., 2015, MNRAS, 454, 3073
Taddia F. et al., 2015, A&A, 574, A60
Takahashi K., Yoshida T., Umeda H., 2013, ApJ, 771, 28
Tanaka M., Hotokezaka K., 2013, ApJ, 775, 113
Tanaka M., Mazzali P. A., Stanishev V., Maurer I., Kerzendorf W. E., Nomoto K., 2011, MNRAS, 410, 1725
Tanaka M. et al., 2016, ApJ, 819, 5

Tauris T. M., van den Heuvel E. P. J., 2006, in Lewin W., van der Klis M., eds, Compact Stellar X-ray Sources. Cambridge Univ. Press, Cambridge, p. 623
Tauris T. M., Langer N., Moriya T. J., Podsiadlowski P., Yoon S.-C., Blinnikov S. I., 2013, ApJ, 778, L23
Tauris T. M., Langer N., Podsiadlowski P., 2015, MNRAS, 451, 2123
Tominaga N., Umeda H., Nomoto K., 2007, ApJ, 660, 516
Umeda H., Nomoto K., 2005, ApJ, 619, 427
Vanbeveren D., Mennekens N., 2015, in Hamann W. R., Andreas S., Helge T., eds, Wolf-Rayet Stars, Universitätsverlag Potsdam, p. 217
Wheeler J. C., Levreault R., 1985, ApJ, 294, L17
Woosley S. E., Heger A., 2015, ApJ, 810, 34
Woosley S. E., Eastman R. G., Weaver T. A., Pinto P. A., 1994, ApJ, 429, 300
Yaron O., Gal-Yam A., 2012, Publ. Astron. Soc. Pac., 124, 668
Yoon S.-C., 2015, Proc. Astron. Soc. Aust., 32, e015
Yoon S.-C., Woosley S. E., Langer N., 2010, ApJ, 725, 940
Zdziarski A. A., Mikołajewska J., Belczyński K., 2013, MNRAS, 429, L104

This paper has been typeset from a TEX/LATEX file prepared by the author.